

The Optical Spectra of Hydrogen Plasma Smelting Reduction of Iron Ore: Application and Requirements

Henri Pauna,* Daniel Ernst, Michael Zarl, Isnaldi Rodrigues de Souza Filho, Michael Kulse, Ömer Büyükuslu, Matic Jovičević-Klug, Hauke Springer, Marko Huttula, Johannes Schenk, Timo Fabritius, and Dierk Raabe

Due to the ever-increasing demand for high-quality steel and the need to reduce CO₂ emissions, research and development of sustainable steelmaking processes have gained a lot of interest in the past decade. One of these processes is the hydrogen plasma smelting reduction (HPSR), which has proven to be a promising solution for iron ore reduction where water vapor is formed instead of CO₂. However, due to the highly dynamic and sometimes unpredictable behavior of plasmas and their nonlinear interaction with the liquid oxides, the monitoring and control of the underlying processes must be improved. This article explores the usage of optical emission spectroscopy (OES) and image analysis for HPSR process monitoring at laboratory and pilot scale. The results cover the time evolution of the OES and camera data with the focus on the most interesting radiating species, such as atomic hydrogen, iron, and oxygen together with the FeO molecule. In addition, the advantages, disadvantages, and requirements of these methods for HPSR process monitoring are discussed.

iron ore with carbon-based reduction in blast furnaces.^[3] However, the EAF route alone cannot solve the reduction of CO₂ emissions due to the continuously increasing demand for steel and decreasing quality of the recycled scrap (which is mostly contaminated postconsumer scrap). Thus, alternative iron ore reduction processes, such as H₂-based direct reduction, are intensively investigated. One of the most known initiatives around this topic is the HYBRIT project, where hydrogen gas is used in a static shaft furnace to reduce solid iron ores.^[4] This is a process referred to as hydrogen-based direct reduction. The process uses hot hydrogen gas that does not contain much excited free radicals, except those few that are provided by thermal activation alone. This means that the kinetics of hydrogen-based direct reduction is in

part determined by the dissociation of the H₂ molecules into atomic hydrogen and the comparably low driving force for the reduction of iron oxide by them.

The hydrogen plasma smelting reduction (HPSR) approach brings the H₂ gas into a plasma state with electricity. In equilibrium, this process can be described by the Saha–Boltzmann distribution and the energy input provided by the electric arc. The resulting hydrogen radicals in the plasma are more reactive than hydrogen gas in direct reduction and have a much higher driving force to reduce the iron oxide (which can in principle be in solid

1. Introduction

The steel industry accounts for ≈7–8% of the global CO₂ emissions, which has created a need for immediate actions to reduce the CO₂ emissions by optimization of the existing processes and implementation of alternative sustainable production routes, such as hydrogen-based and electrified reduction methods using renewable energy.^[1] Today, around 40% of European steel is produced via the electric arc furnace (EAF) route using steel scrap,^[2] resulting in 77% lower CO₂ emissions than producing steel from

H. Pauna, T. Fabritius
Process Metallurgy Research Unit
University of Oulu
P.O. Box 4300, FI-90014 Oulu, Finland
E-mail: henri.pauna@oulu.fi


D. Ernst, M. Zarl
K1-MET GmbH
Stahlstraße 14, A-4020 Linz, Austria

I. R. Souza Filho, M. Kulse, Ö. Büyükuslu, M. Jovičević-Klug, H. Springer, D. Raabe
Max-Planck-Institut für Eisenforschung
Max-Planck-Str. 1, 40237 Düsseldorf, Germany

H. Springer
Institut für Bildsame Formgebung
RWTH Aachen University
Intzestrasse 10, D-52056 Aachen, Germany

M. Huttula
Nano and Molecular Systems Research Unit
University of Oulu
P.O. Box 3000, FI-90014 Oulu, Finland

J. Schenk
Department of Metallurgy
Chair of Ferrous Metallurgy
University of Mining Leoben
Montanuniversität Leoben, 8700 Leoben, Austria

 The ORCID identification number(s) for the author(s) of this article can be found under <https://doi.org/10.1002/srin.202400028>.

© 2024 The Authors. Steel Research International published by Wiley-VCH GmbH. This is an open access article under the terms of the Creative Commons Attribution License, which permits use, distribution and reproduction in any medium, provided the original work is properly cited.

DOI: 10.1002/srin.202400028

or in liquid state). This means that some of the chemical energy entering the process through the H_2 in conventional hydrogen-based direct reduction is replaced by electrical energy in HPSR processes, equipping the redox process with reactive hydrogen radicals. This implies that the plasma-based approach turns the reduction into a partly electrified chemical reaction, with the aim to balance the use of (indirect) chemical energy with the use of (direct) sustainable electrical energy.^[5,6]

For this reason, HPSR has been studied extensively during the past two decades both in laboratories and in pilot scale. Seftjani et al.^[7] described the thermodynamics of liquid iron ore HPSR and how the hydrogen species affect the reduction, with the conclusion of $H^+ > H_2^+ > H_3^+ > H > H_2$ as the optimal species for HPSR. This relation creates a favorable reduction environment for the thermal hydrogen plasma, where atomic and ionized species are present.^[8] Plaul et al.^[5] studied the physical and chemical fundamentals of HPSR, where they reduced iron ore in H_2/Ar plasma and reached near 100% reduction degree in ≈ 1600 and 2300 s with 50% and 30% H_2 , respectively. They noted that hydrogen utilization degree decreases with increasing hydrogen content. As low as 10% hydrogen content has been observed to be sufficient to fully reduce hematite, as shown in the work of Souza Filho et al.^[9] They observed that a larger molten oxide bath facilitates the transport of oxygen to the reduction reaction zone. In comparison to shaft furnace solid-state direct reduction of iron ore with gaseous hydrogen, they found out that the HPSR with 10% H_2 partial pressure yielded comparable reduction rates.

Due to the complex behavior of plasmas, one of the most important perspectives for the future advancement of HPSR is to create a profound process control. Zarl et al.^[10] defined stability fields for the HPSR process, identifying several factors, such as hydrogen and argon content, the gas mixture's relation to the required electrical input, and ore charging, that have a significant effect on the stability of the plasma. In addition, several reactor and material-related parameters have been studied, including optimization of the prereduction degree of the iron ore,^[11,12] the feed material charging rate,^[13,14] slag formation and composition,^[15] hydrodynamics and hydrogen flow rate,^[16] and both the shape and quality of the electrode.^[17] To advance the process control and monitoring of HPSR, investigation and implementation of new methods are essential. Optical emission spectroscopy (OES) has proven to be a suitable measurement method at EAFs and ladle furnaces to assess characteristics of the plasma, molten bath temperature, and slag composition.^[18,19] Due to the similarities between EAF steelmaking and HPSR, the experience from the EAF OES analysis can be used as a foundation for the HPSR analysis.

These works show that some of the principles of HPSR have been studied for several years. However, it is important to develop new monitoring methods and use them for better process control to reach higher material and energy efficiency. To this end, this article presents OES data coupled with plasma images obtained on two laboratory reactors and one pilot-scale reactor. The results provide information on what kinds of insights the OES spectra hold for the hydrogen plasma-based iron ore reduction and links the spectra to the colors of the plasma. The findings focus on 1) determining the most important species that can be identified from the spectra related to the

HPSR, 2) creating knowledge of what can be inspected from the colors of the plasma by visual and optical inspection, and 3) discussing the advantages and requirements of the OES as an analysis method.

2. Experimental Section

The HPSR measurement campaigns were performed at the Max-Planck-Institut für Eisenforschung GmbH (MPIE), Montanuniversität Leoben (MUL), and K1-MET GmbH. Each facility was equipped with a unique HPSR reactor, allowing to assess the process' physical and metallurgical aspects from laboratory up to pilot scale. To ensure as stable plasma behavior as possible, the plasma length was manually changed in all three facilities. A schematic presentation of the reactors and the OES measurement setups is presented in Figure 1. The reactor specifications are listed in Table 1. The experimental conditions vary in each of these reactors, and the purpose of using three reactors was to better understand how the HPSR process behaves at different circumstances.

As illustrated in Figure 1, the optical fibers' solid angles encapsulated different parts of the plasma and the reactor. At MPIE and MUL, the flange limited the direct light to be observed at around a 4 cm-diameter section of the plasma, electrode, and crucible. At K1-MET, light was received at a larger area due to the longer distance between the fiber and the plasma, and thus light came from the plasma, electrode, and crucible of the reactor. Due to thermal radiation, molten surface created a continuous background to the spectra. Ambient light did not reach the spectrometer because there were no intensive light sources nearby and due to low slit width of $10\ \mu\text{m}$. However, the molten surface and the walls of the furnace may cause light reflections. At MPIE, the reactor's wall was not in the narrow solid angle

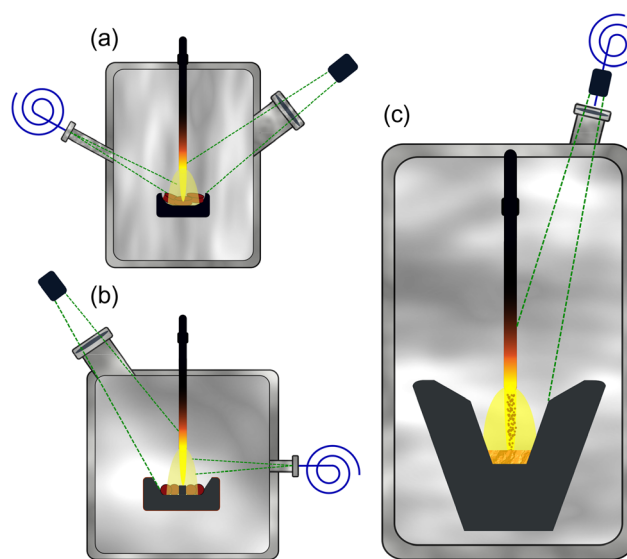


Figure 1. Schematic illustration of the HPSR reactors and measurement setups at a) MPIE, b) MUL, and c) K1-MET. The camera is marked with a dark box, optical fiber with an enfolded blue line, and the approximative view cones into the reactors with dashed green lines. The camera and optical fiber monitor the plasma through the same window at K1-MET.

Table 1. Reactors' specifications.

Facility	Max. capacity [g]	Weight range of samples	Crucible	Crucible diameter [cm]
MPIE	30	15 g hematite	Copper	5
MUL	200	20–97 g iron ore	Steel	10
K1-MET	90 000	1500 g iron ore, 100–200 g min ^{−1}	Refractory	25

of the optical fiber. At MUL and K1-MET, the reactors' walls that were visible to the optical fiber were porous refractory material, causing less reflection to the spectra in comparison to well-reflecting material. It was observed that the effect of reflection to the spectra was negligible, but it should be noted that reflections may cause systematic error up to a few percents to, for example, the absolute values of plasma temperature and electron density. The measurement setups represent the likely scenarios that will be faced in larger reactors built for industrial purposes, allowing to assess the methods' performance and scalability to larger reactors.

High-purity lab-grade hematite compacts, prepared from hematite ore powder, were placed directly on the water-cooled copper hearth of the reactor at MPIE. Before the experiments, the air in the reactor chamber (18 L) was evacuated and purged with Ar. For the reduction experiments, the reactor was filled with a gas mixture of 90%Ar-10%H₂ up to an absolute pressure of 900 mbar. The plasma was ignited with a current of around 200 A by manually contacting the electrode with the Cu hearth and bringing the plasma on top of the hematite compact. The plasma length varied between 1 and 2 cm. The material was simultaneously melted and reduced for ≈120 s under the hydrogen-containing plasma. Then, the plasma was switched off, and the reactor was replenished with a fresh gas mixture of 90%Ar-10%H₂ because the hydrogen is consumed in the reduction process. The experiments continued in ≈60 s steps up to 640 s total reduction time and the chamber was always replenished after each step to provide sufficient stoichiometry for the continuation of the reactions.

For the batch material at MUL, iron ore pellets were added to the crucible. The total iron content of the pellets was 67% with Al₂O₃, SiO₂, CaO, MgO, TiO₂, K₂O, and Na₂O as notable gangue elements (from 0.05% up to 1% each). The reactor was first purged and filled with Ar gas through a hollow electrode (HGE). The plasma was ignited with contact between the electrode and the crucible's ignition pin. The plasma length and current were changed between 3 and 5 cm and 80 and 160 A, respectively. The iron ore batch was melted with 100% Ar plasma. When the melt was formed, H₂ was introduced into the chamber through the HGE with a target gas atmosphere of 3:2 Ar:H₂ with Ar and H₂ gas flow rates of 3 and 2 L min^{−1}, respectively. The total gas flow rate was kept at 5 L min^{−1}. When the desired state was reached or the power supply started to critically heat up, the power was switched off.

The HPSR campaign at K1-MET was started with a 9500 g batch of premelted steel chips. The chamber was purged with Ar gas and the plasma was ignited with a contact between the electrode and the steel chips. The plasma length was kept between 15 and 18 cm. The premelt was exposed to 300 L min^{−1} Ar plasma for 420 s followed by 300 s of 200:200 L min^{−1} Ar:H₂ plasma at 500 A. After this, fine iron ore fines were continuously charged through the HGE in four separate experimental steps. The total iron content of the fines was 66% with C, TiO₂, Al₂O₃, P₂O₅, MnO, SiO₂, and TiO₂ as notable gangue elements (from 0.05% up to 1.5% each). The experimental details for MPIE, MUL, and K1-MET are listed in Table 2.

At MPIE, an Andor Solis SR-500 Czerny-Turner spectrometer with a water-cooled Newton DU940N charge-coupled device

Table 2. Experimental details for the reduction experiments ("E" in the table). Premelting at MUL was done under pure Ar flow. The K1-MET campaign started with a 9500 g premelted steel chip batch before the campaign. The premelt was then exposed to 400 L min^{−1} Ar:H₂ plasma at 500 A. At MPIE, no premelting of input ore was made. MPIE: Max-Planck-Institute für Eisenforschung GmbH; MUL: Montanuniversität Leoben; K1-MET: K1-MET GmbH.

MPIE	E	Ar:H ₂	Batch material [g]	I [A]	U [V]	Pre-melting [s]	Reduction time [s]
	1	9:1	15.0 ^{a)} Fe ₂ O ₃	218	22.8	–	640
MUL	E	Ar:H ₂ [L min ^{−1}]	Batch material [g]	I [A]	U [V]	Pre-melting [s]	Reduction time [s]
	1	3:2	96.2 ^{b)} Fe-ore	80–160	30–90	354	585
K1-MET	E	Ar:H ₂ [L min ^{−1}]	Iron ore fines continuous charging	I [A]	U [V]	Post-reduction after charging [s]	
	1	200:200	100 ^{c)} g min ^{−1} , 6 min	495–503	108–144	540	
	2	200:200	100 ^{c)} g min ^{−1} , 1 min	482–495	149–244	180	
	3	200:200	100 ^{c)} g min ^{−1} , 3 min	492–494	103–195	540	
	4	100:100	200 ^{c)} g min ^{−1} , 1 min 100 ^{c)} g min ^{−1} , 3 min	392–398	97–106	0	

^{a)}Disk. ^{b)}Pellet. ^{c)}Fines.

(CCD) camera was used to record the optical emissions from the plasma with 11 spectra s^{-1} and integration time of 80 ms. An Ocean Optics QP600-2SR optical fiber was used to collect the light. The CCD was cooled down to -45°C to decrease the dark current with water-cooled Peltier element. A 300 lines mm^{-1} grating was used to cover 279.39–645.00 nm. The region near 656 nm was intentionally cut out from the wavelength coverage due to the highly intensive H_{α} line that would have obstructed the analysis of the weaker lines around it. An Imperx CCD BobCat single-lens reflex camera with 2456×2058 pixel resolution was used to record videos of plasma. Camera observations of the reactor were conducted through a 1 cm-thick glass flange. The distance between the camera and the glass was 200 mm, and the distance to the plasma was 400 mm. A framerate of 11 images s^{-1} was used with an exposure time of 112 μs . The camera was equipped with an FBH380-10 bandpass filter from Thorlabs. The filter's wavelength range was centered at 380 with a 10 nm full width at half maximum (FWHM). This filter was chosen because intense optical emission lines from atomic iron resided in this region and were the main intensity contributors within the wavelength range.

At MUL and K1-MET, a three-channel spectrometer from Avantes BV composed of three AvaSpec-ULS3648-USB2-RM spectrometers was used to cover the 300–1040 nm wavelength range. The exposure time was changed from 30 μs up to 50 ms depending on the visibility of the plasma. The camera used in both facilities was Axis-Q1775 with 1024×768 pixel resolution from Pieper GmbH, Schwerte, Germany. The exposure time was automatically adjusted based on the visibility and brightness of the plasma. To ensure a good white balance and that the camera captures both the brightest and the darkest parts of the process, a wide dynamic range mode was activated. The camera was configured with two additional filters. The first filter was an IR filter type FRO7012 from Pieper GmbH for reactor chamber observations with a thickness of 2 mm. The second filter was a gold-plated disc from Pieper GmbH with 30% remaining permeability and a 2.5 mm thickness. Red, blue, yellow, and orange colors were analyzed from the images with different pixel color thresholds for red, green, and blue (RGB). The standard RGB pixel values ranged from 0 to 255, and the color thresholds are given in Table 3. More details of the spectrometer and the MUL reactor can be found in Ref. [20].

3. Theory

The optical emissions of plasma are characterized by unique spectral lines that arise from the excitation-relaxation reactions of the particles within the plasma volume. These optical

Table 3. RGB pixel color thresholds to analyze red, blue, yellow, and orange colors in the images.

Color	Red pixel	Green pixel	Blue pixel
Red	>230	<210	>170
Blue	<170	>220	>190
Yellow	>200	>210	<160
Orange	<230	>150	<100

emissions hold information on the composition of plasma and can be used to characterize its physical properties. Four magnified spectrum examples are displayed in Figure 2 for the MUL reactor. The atomic optical emissions in a–c are derived from the NIST atomic spectra database.^[21] The notations I and II describe a neutral and singly ionized species, respectively. Figure 2a comprises iron, hydrogen, and ionized calcium, whereas chromium and magnesium around 515–521 nm together with sodium near 589 nm can be observed in b). Alkali lines, such as the Na doublet near 589 nm, occur due to the existence of minor volatile gangue-related impurities in the feedstock ores. Most of the argon lines reside above 700 nm, as shown in c). In addition, molecular optical emissions from FeO can be observed occasionally, especially during the beginning of the reduction process. These molecular emissions form a broadband structure from 550 to 650 nm with intensity maxima near 565, 590, and 625 nm, as shown in Figure 2d. This band structure, as highlighted in Figure 2d, has also been observed by Julien et al. in flame spectra.^[22]

The plasma temperature and electron density were evaluated from the OES spectra with Boltzmann equation and FWHM of the hydrogen lines, respectively. The equations have been described in a previous publication related to H_2 -plasma OES study.^[20] Fe I optical emission lines were used in the Boltzmann equation, and the optical emission line-specific details for wavelength (λ_{mn}), transition probability (A_{mn}), upper energy level (E_m°), and upper energy level degeneracy (g_m) are listed in Table 4. Indices m and n refer to upper and lower energy level, respectively, and z to the ionization degree. Only the plasma temperatures that yielded $R^2 > 0.90$ in the Boltzmann equation plot are considered.

To obtain an estimate on how the electron density evolves during the HPSR process, the electron densities were evaluated using empirical formulae describing the relation between H_{α} and H_{β} optical emission lines' FWHM and electron density, where the experimental constants for H_{α} and H_{β} were provided in the work of Surmick et al.^[23] H_{α} was used for MUL and K1-MET, and H_{β} for MPIE. An alternative method to determine the electron density is to use, for example, the Saha-Boltzmann equation, requiring optical emissions from two sequent ionization degrees, such as neutral (I) and singly ionized (II). Identification of frequently present ionized species, such as Fe II, is under investigation by the authors for future research.

4. Results and Discussion

4.1. Laboratory Campaigns

4.1.1. MPIE

Figure 3 depicts 11 examples of the plasma images acquired through the bandpass filter together with spectra recorded in the wavelength range between 350 and 500 nm for the course of HPSR of hematite disks at MPIE. The bandpass filter's coverage is in between the vertical dashed lines displayed in the spectra of Figure 3, consisting mainly of Fe I. Thus, the heat map-like images depicted in Figure 3 show the atomic iron radiating within the observed system. The warmer colors in this figure indicate brighter optical emissions from Fe I in a particular

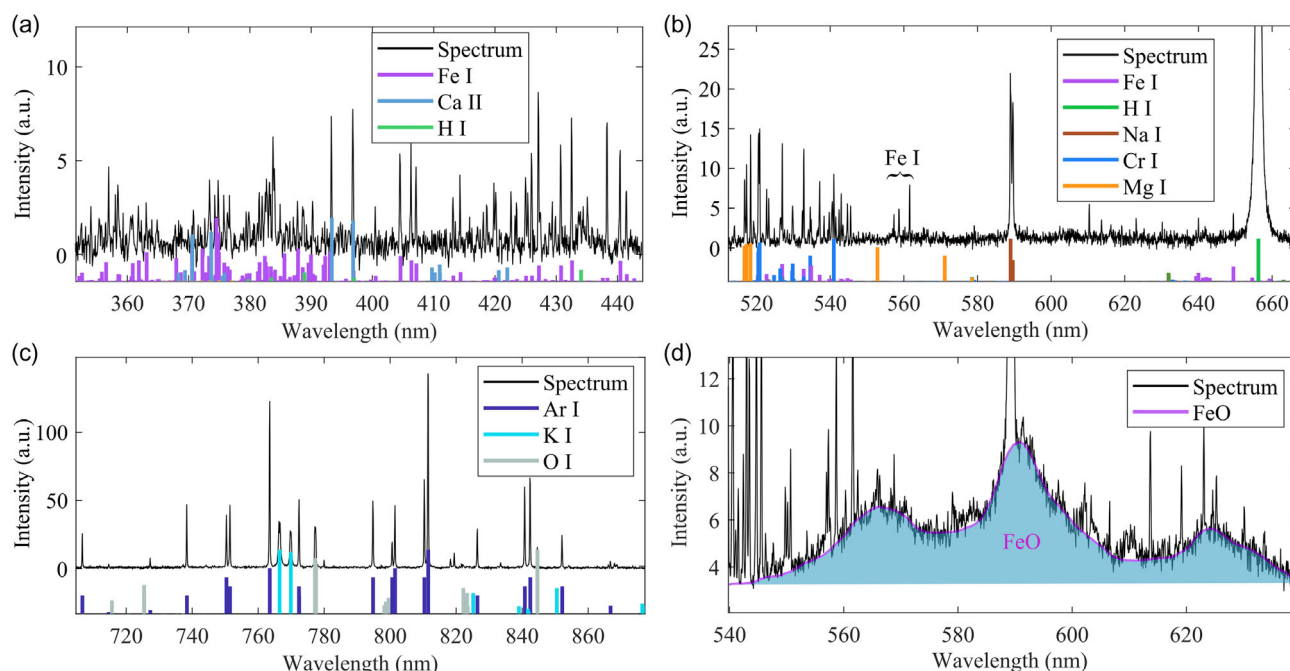


Figure 2. Spectra in the MUL experiment from a) 350 to 445 nm, b) 515 to 665 nm, and c) 705 to 870 nm from H_2/Ar plasma, and d) 540 to 640 nm at the start of the reduction. The atomic optical emission lines are derived from the NIST atomic spectra database.^[21]

Table 4. Fe I optical emission lines used for plasma temperature analysis.

λ_{mn} [nm]	A_{mn} [s^{-1}]	E_m^z [eV]	g_m
426.047	3.99e+07	5.31	11
442.731	3.41e+04	2.85	9
446.165	2.95e+04	2.87	7
446.665	1.20e+07	5.61	7
447.608	1.01e+07	5.61	5
448.217	2.09e+04	2.88	5
452.861	5.44e+06	4.91	9
495.760	4.22e+07	5.31	11
513.946	8.69e+06	5.35	9
516.749	2.72e+06	3.88	7
517.160	4.46e+05	3.88	9
522.719	2.89e+06	3.93	5
523.294	1.94e+07	5.31	11
527.036	3.67e+06	3.96	3
528.362 ^{a)}	1.02e+07	5.59	7

^{a)}Not used in MPIE analysis.

region. The spectra show also the broad H_β and H_γ lines at 486 and 434 nm, respectively, which do not contribute to the light in the plasma images. The plasma core has an abundance of atomic iron, and a dimmer sheath is also observed at the edges of the plasma, suggesting partial evaporation of the melt. Due to the high instability of the plasma and evaporation rate of material during the first 20 s after the plasma ignition, especially driven

by the thermal decomposition of hematite, the first plasma image is displayed at plasma ignition and the following images in 60 s intervals. At plasma ignition, solid hematite rapidly evaporates into the plasma. Within 60 s after ignition, hematite has melted, and the plasma has stabilized. The glow lying below the plasma in Figure 3c–k originates from the melt surface that starts to glow around 120 s of reduction. Identifying the origin of the glow will be covered in a future project of the authors, as this glow could be either the reflection of the plasma from the molten pool or actual atomic iron radiating on the melt surface (reduced iron floating near the surface of the oxidic melt).

To illustrate how different species radiate within the plasma over time, **Figure 4** shows the time evolution of Ar I intensity and intensity ratios for $\text{H}_\beta/\text{Ar I}$, $\text{FeO}/\text{Ar I}$, and $\text{Fe I}/\text{Ar I}$ together with the plasma images' pixels' brightness, plasma temperature, and estimated electron density in the MPIE experiment. The intensity of argon varies due to the movement of plasma during the HPSR process. Since the argon content in the reactor remains approximately constant during the process, optical emission intensities of H_β , FeO , and Fe I documented in Figure 4 have been divided by the intensity of Ar I to remove the effect of varying overall spectrum intensity due to movement of the plasma and adjustment of the electrode.

All the variables displayed in Figure 4 remain relatively stable over the first 90 s, except for the Ar I and camera intensities together with electron density at 50 s. At this point, the reactor's operator manually moved the electrode, which is necessary to maintain stable plasma above the melt, increasing the length of the arc. At 90 s, the $\text{Fe I}/\text{Ar I}$ and $\text{FeO}/\text{Ar I}$ intensities increase, and plasma temperature rises from around 4800–5100 K. It can be seen in Figure 3b,c that the melt surface has started to glow

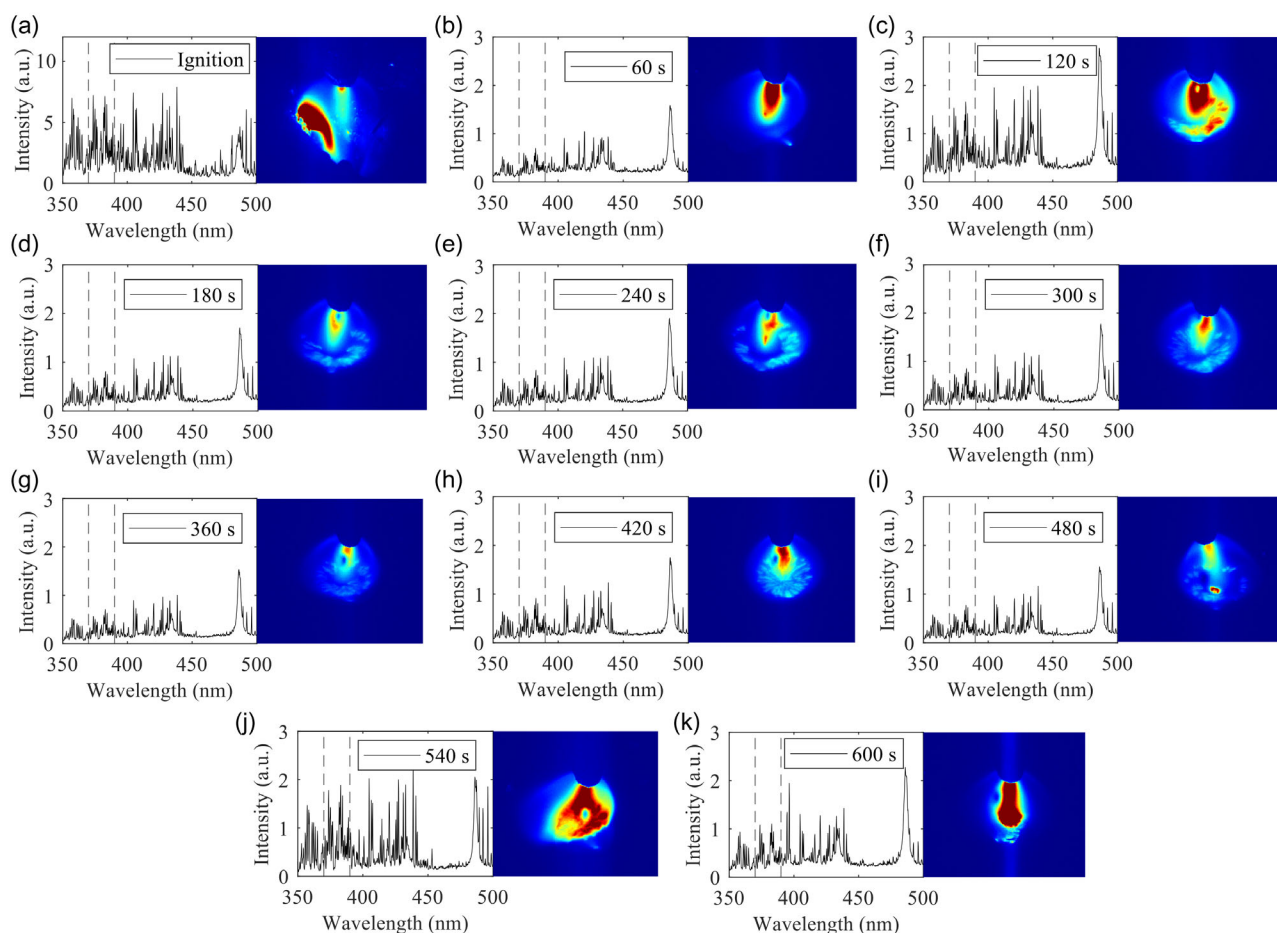


Figure 3. Spectra and images at a) plasma ignition, b) 60 s, c) 120 s, d) 180 s, e) 240 s, f) 300 s, g) 360 s, h) 420 s, i) 480 s, j) 540 s, and k) 600 s from the start of the MPIE experiment. The bandpass filter's wavelength range is between the dashed lines in each spectrum.

from 90 s point onward, possibly indicating metallic iron on the melt surface.

The most significant changes can be observed after 390 s when both the Fe I/Ar I ratio and the camera image brightness increase first at the beginning of the individual experiment steps and then from 580 s until the end of the experiments. At around 480 s, and from that point onward, a bright spot emerges in the plasma images onto the melt surface, as illustrated in Figure 3i. Here, pure metallic iron droplets could be visually detected on the melt through the viewport of the reactor. This fact provides strong evidence that the highly concentrated Fe domains underneath the plasma can be attributed to the nucleation of metallic iron inside the oxidic liquid. From 575 s onward, the images are saturated by Fe optical emissions in the plasma core, as shown in Figure 3j,k.

To quantify the metallization of the samples, the same HPSR procedure was performed separately for similar 15 g hematite disks for 2 and 5 min. The metallizations of the samples at 2, 5, and 10 min were 2%, 40%, and 92%, respectively. When comparing these results to the time evolution of Figure 4, the increase of both the image brightness in e) and the Fe I/Ar I optical emission intensity ratio in d) between 390 and 640 s could be used as indicators of formation of metallic iron on the melt

and to monitor the later stages of the reduction. This is essential for process development, since stopping the process at full metallization can prevent material losses caused by evaporation and increase energy efficiency.

4.1.2. MUL

In the MUL experiment, iron ore pellets were charged to the crucible and melted under a pure Ar plasma atmosphere. **Figure 5** shows nine example spectra and plasma images from this experiment. The H_{α} line at 656 nm can be seen even under pure argon flow in Figure 5a–d. The H_{α} most probably originates from moisture and residual H_2 in the atmosphere from the previous HPSR experiment. H_2 is introduced into the reactor at 500 s and the plasma color gets a red hue from the H_{α} optical emission. From this point onward, the reduction reaction starts, and the overall OES intensity drops, as seen in Figure 5f–i. At f) and h), the plasma color clearly has blue and yellow colors, originating from Fe I and FeO, respectively. There is also notable water vapor and dust formation during the reduction, as seen in Figure 5h, where the dust and vapor create a yellow and orange hue around the plasma. The spectrum intensity increases toward

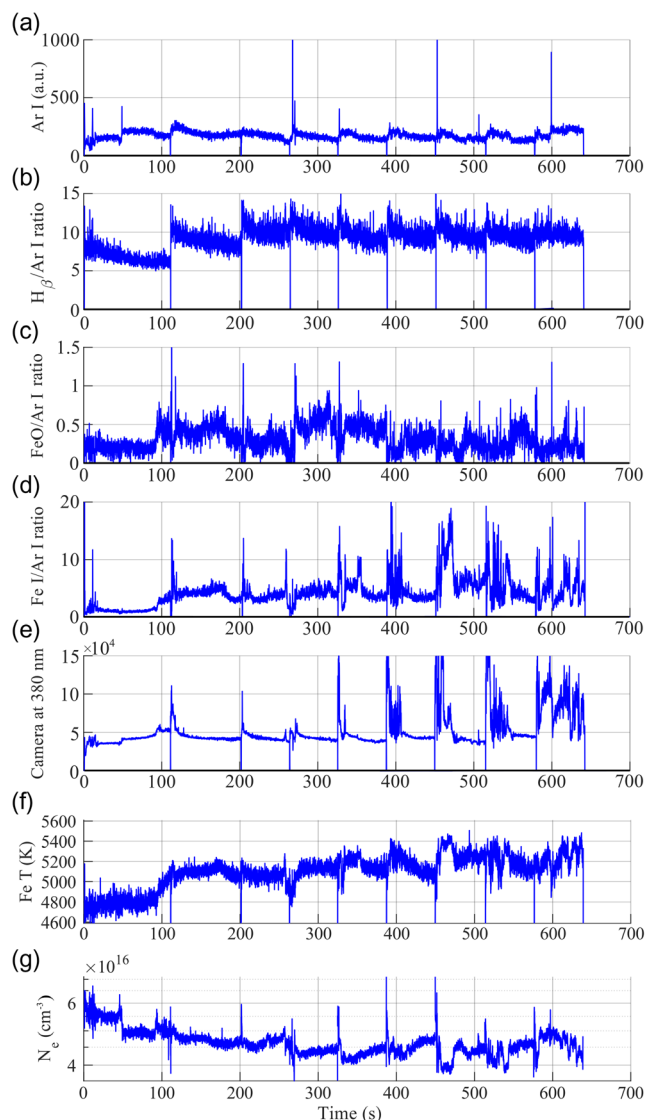


Figure 4. Time evolution of a) Ar I intensity and intensity ratios for b) $H_{\beta}/Ar\ I$, c) $FeO/Ar\ I$, d) $Fe\ I/Ar\ I$, together with e) sum of the plasma images' pixels' brightness, f) Fe plasma temperature, and g) estimation of the electron density with H_{β} in the MPIE experiment. The experiments were conducted in nine separate steps, between which the values drop to zero.

the end of the experiment, as documented in Figure 5i, where optical emissions from CaO and Na I together with minor FeO can be seen near the yellow and red parts of the spectrum of light. The optical emissions from CaO were identified from the MUL HPSR spectra in a previous study.^[20] This spectral region is shown more clearly in Figure 6, where the notable band maxima are \approx at 555 and 625 nm for CaO, and 565, 590, and 625 nm for FeO.

Figure 7 shows the time evolution of H_{α} , O I, Fe I, Ca II, CaO, and Na I in addition to red, blue, and orange pixel intensities of the camera images and plasma characteristics. As seen in Figure 5, the overall spectrum intensity varies a lot depending on the absorption of light by dust. For example, only the most intensive emission lines are observable in Figure 5h. In contrast

to MPIE, the spectra at MUL and K1 were normalized to the sum over the entire spectrum instead of Ar I line due to lack of Ar I lines at these instances. Thus, the OES line intensities in Figure 7 have been normalized with the total spectrum intensity to remove the fluctuation of the overall intensity due to the movement of the plasma.

From the start of the experiment, signals can be observed for all these species except for CaO. In Figure 7b, Fe I optical emissions' most intensive occasions correspond well to the increasing blue color brightness in the plasma images, as illustrated in Figure 5c. At these instances, plasma temperature increases, and electron density decreases even though metallic vapor in the plasma usually increases the electron density. Here, the electron density decreases due to increasing plasma length caused by plasma movement from the center of the crucible to its sides where there are still unmolten pellets. Examples of plasma at the center and side of the crucible are displayed in Figure 5d,c, respectively.

The red pixel, H_{α} , and O I intensities increase significantly after the addition of H_2 at 500 s. Since the only significant source of oxygen is molten oxide, the increasing O I optical emissions are related to the reduction of the melt. Afterward, H_{α} and O I intensities gradually decrease over time from 800 s onward to near-zero values, where a lower O I intensity may be attributed to decreasing reduction rate. However, the overall spectrum intensity is very low due to absorption of light by dust after 800 s, as shown in Figure 5h. Even though H_{α} and O I intensities remain relatively low at the later stages of the experiments, optical emissions from other species can be clearly seen in Figure 5i at 1028 s. Figure 7b,c reveal that orange pixel, Ca II, CaO, and Na I intensities increase from 900 s onward. This, in turn, suggests that a slag-like layer from the residual gangue elements contained in the original iron ore has formed on top of the melt. Since the purpose of this experiment was to study how OES could be used to monitor the HPSR process, the metallization degree and slag analyses were not performed, and these topics will be studied in future experiments.

It should be noted that the overall intensity of the spectra steadily decreases after 800 s, and the spectrum intensity is considerably low after 1000 s where the spectrometer occasionally does not receive enough light due to absorption. When comparing the pixel intensities with the spectra, the camera images are well seen during the reduction, but the intensities of the OES spectra drop drastically. The integration time of the spectrometer was increased several times from 30 μ s up to 50 ms during reduction, but it was not always sufficient for the spectrometer to receive enough light for proper spectral analysis. To increase the amount of light arriving to the spectrometer's detector during dust formation, a wider slit should be tested to mitigate the effect of light absorption by the dust.

4.2. Pilot-Scale Campaign

The campaign at the K1-MET HPSR pilot-reactor consisted of four separate experiments where iron ore was continuously charged through the HGE. These four experiments' general characteristics are relatively similar; thus, one exemplary experiment with spectra and plasma images is explained here. Nine spectra and images from experiment 4 with 100 g min⁻¹ iron ore fines

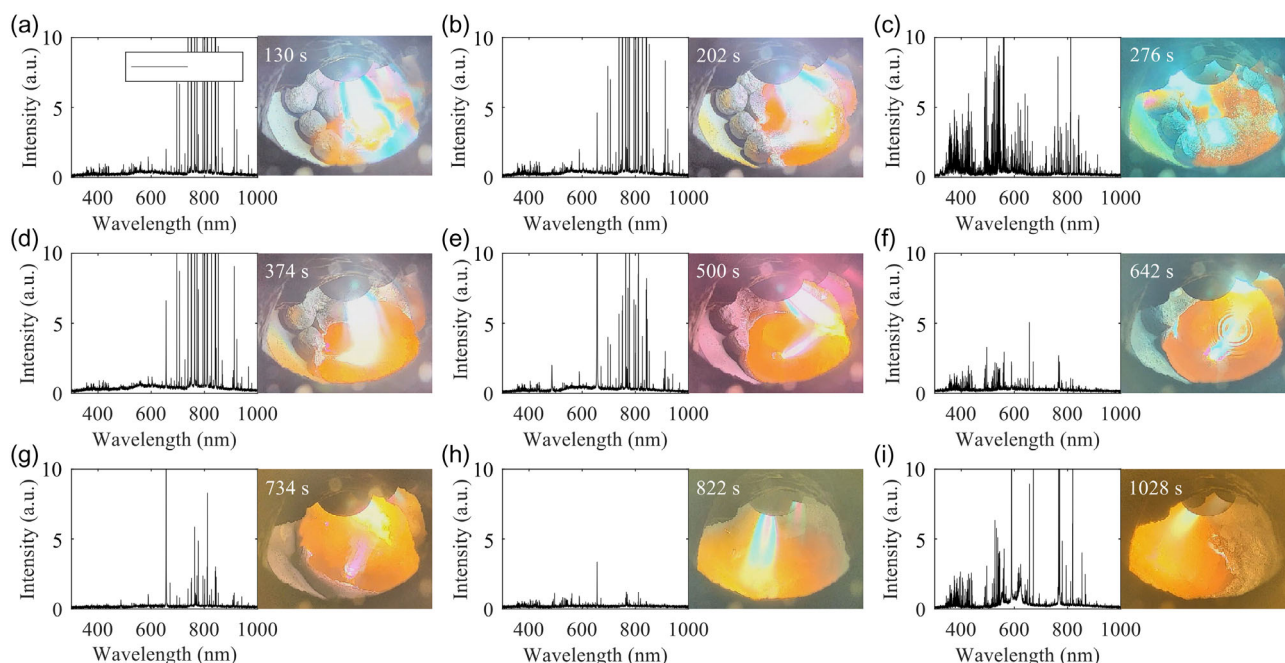


Figure 5. Spectra and images at a) 130 s, b) 202 s, c) 276 s, d) 374 s, e) 500 s, f) 642 s, g) 734 s, h) 822 s, and i) 1028 s from the start of the MUL pellet batch experiment.

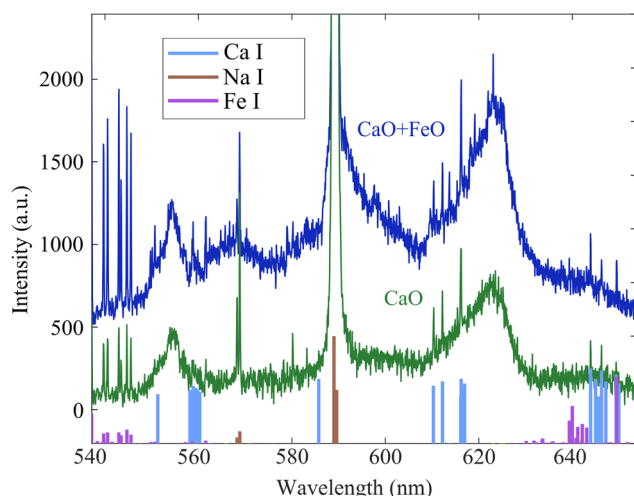


Figure 6. Two spectra with optical emissions from CaO + FeO (upper) and only CaO (lower). An offset of 500 a.u. has been applied to the CaO + FeO spectrum for better readability. The atomic optical emission lines are derived from the NIST atomic spectra database.^[21] The spectra have been adjusted so that the CaO and FeO optical emissions are clearly visible, and thus the intensities of the Na I lines are not fully displayed in this figure.

feed for 3 min are displayed in **Figure 8**. Image and spectrum in a) are 10 s before the charging starts and b) at the start of charging. When comparing the spectra, there is a significant increase in the overall spectrum intensity when the iron ore fines enter the plasma, and no dust or water vapor obstructs the view. The broad structure in the spectrum b) from 500 to 620 nm is

molecular optical emission from FeO, whereas the background consists of continuum and thermal radiation. Spectral analysis reveals that the spectrum in b) is dominated by the Fe I and FeO, whereas atomic hydrogen or argon lines cannot be detected. As the charging progresses in c), the spectra can still be seen when the integration time of the spectrometer is increased from 30 μ s up to 50 ms for the reduction. The charging stops around 180 s, after which the light intensity drops to zero in d) and e). The red glow from the plasma starts to emerge again around 300 s when the intensive red H_{α} line can be seen in the spectra of f–i). Postreduction continues until the end of the experiment before the electrode is lifted in i). As the electrode is raised, the plasma occasionally wanders to the side of the crucible, where there is still solid iron ore. Hence, the image in i) has both blue and yellow glow from atomic iron and FeO, respectively.

From the start of the preparations of the measurement campaign, the plasma was ignited at 780 s. The video recording was initiated at 800 s. **Figure 9** starts from 1500 s and hydrogen is introduced to the reactor at 1550 s, whereupon H_{α} optical emission appears. When comparing the Fe I line intensities with the blue pixels, their highest intensity peaks match each other. Similar to the laboratory reactor, blue light can be attributed to atomic iron radiating in the plasma. However, without iron ore, the yellow glow with pure argon does not correspond to the FeO, but rather to the low-intensity Ar I lines and thermal radiation from the molten bath. Such a spectrum is illustrated in **Figure 8a**.

Similar to **Figure 7** for MUL experiment, **Figure 9** displays the time evolution of OES and image data for K1-MET experiments. The start and end of the four experiments are marked with green and red vertical lines, respectively. Experiments 1 and 2 started at 1975 and 2990 s, respectively, where H_{α} line and Ar intensities drop immediately with an abrupt increase in blue pixel, Fe I,

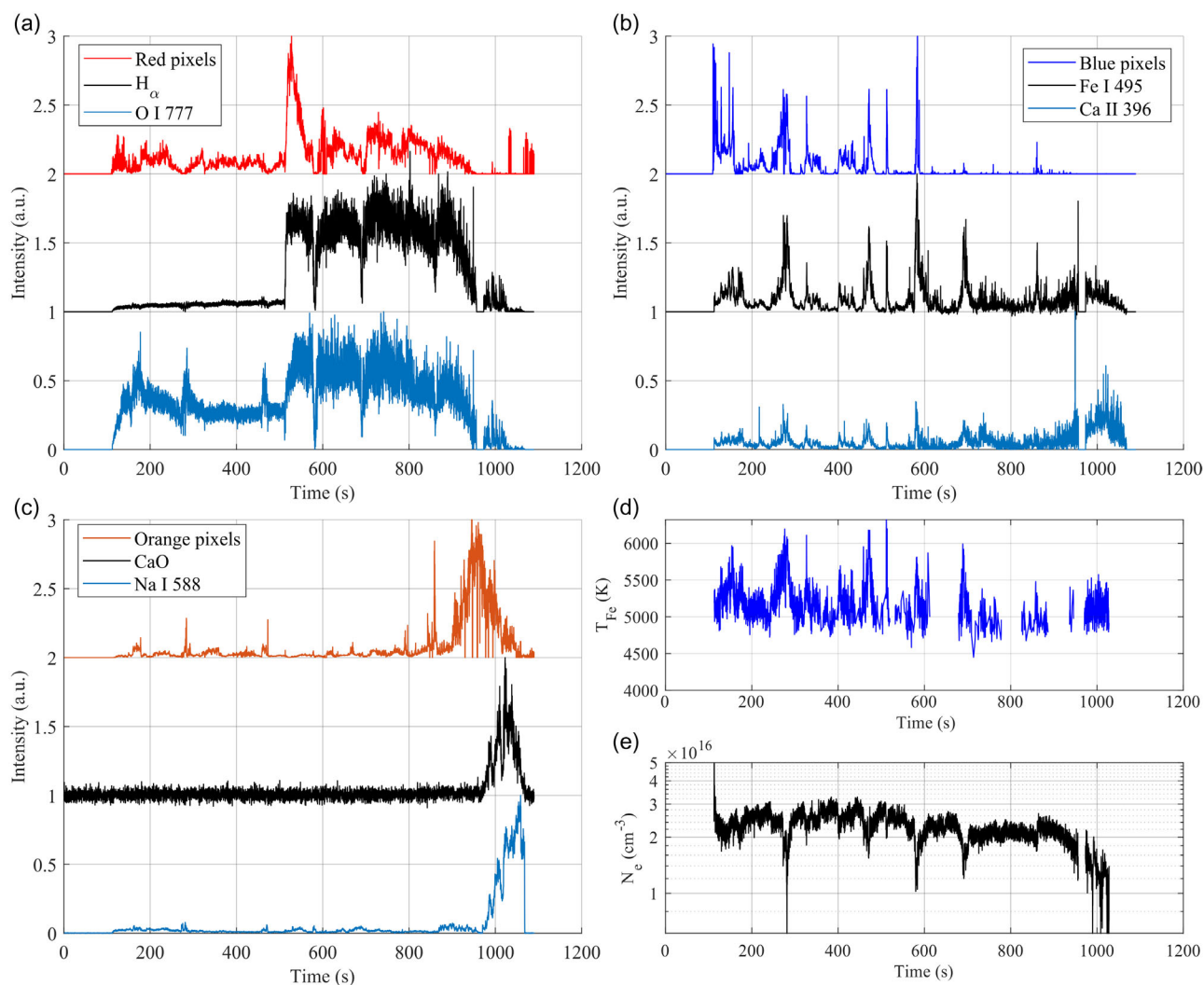


Figure 7. Time evolution of pellet batch reduction experiment at MUL with a) red pixel, H_{α} , and O I intensities, b) blue pixel, Fe I, and Ca II intensities, c) orange pixel, CaO, and Na I intensities, d) Fe plasma temperature, and e) estimation of electron density with H_{α} . The intensities in a–c) have been normalized with respect to the overall intensity of the spectrum and an offset has been applied to the graphs for better readability.

Ca II, and yellow pixel intensities. However, within a few seconds, the spectrum intensity drops to near-zero values rapidly, and no light is received momentarily after the start of the experiment. The camera images of experiment 1 show a significant increase in yellow pixels originating from FeO, whereas blue pixel intensities are higher in experiment 2. The difference between these two experiments is the duration of the charging period and the electrical input. Experiments 1 and 2 had feeding rates of 100 g min^{-1} for 6 and 1 min, respectively, whereas experiment 2 had, on average, double the voltage compared to experiment 1. When comparing the colors of experiments 1 and 2, the blue color is significantly higher in experiment 2, indicating that the fines dissociate into iron atoms at a higher rate than in experiment 1. This is to be expected with higher electrical input.

Experiments 3 and 4 start at 3390 and 4380 s, respectively, in Figure 9. Here, experiment 3 consists of an iron ore fines feed of 100 g min^{-1} for 3 min followed by 200 g min^{-1} for 1 min, whereas experiment 4 uses only half the Ar and H_2 gas flow rates

in comparison to experiments 1–3 with 100 g min^{-1} for 3 min. Similar to the comparison between experiments 1 and 2, more blue light can be observed in experiment 3 than in 4 due to higher electrical input. Between 4000 and 4250 s, the plasma moves occasionally to the sides of the bottom of the crucible where and hits nonreduced iron ore. At these times, the Fe I, O I, FeO, Na I, and yellow pixel intensities increase. Toward the end of experiment 4 at around 4500 s, the OES intensities drop to 0 due to absorption of light by dust. The integration time was manually decreased after experiment 4 when the dust decreased in the atmosphere. At 4710 s, the electrode is lifted in steps to conclude the measurement campaign. The image of the plasma at this time can be seen in Figure 8i.

The plasma temperature fluctuates significantly during and between the experiments. Furthermore, Fe I optical emission intensities are relatively low in these experiments and temperature with high-enough R^2 in the Boltzmann plot cannot always be determined. In the beginning of each continuous charging

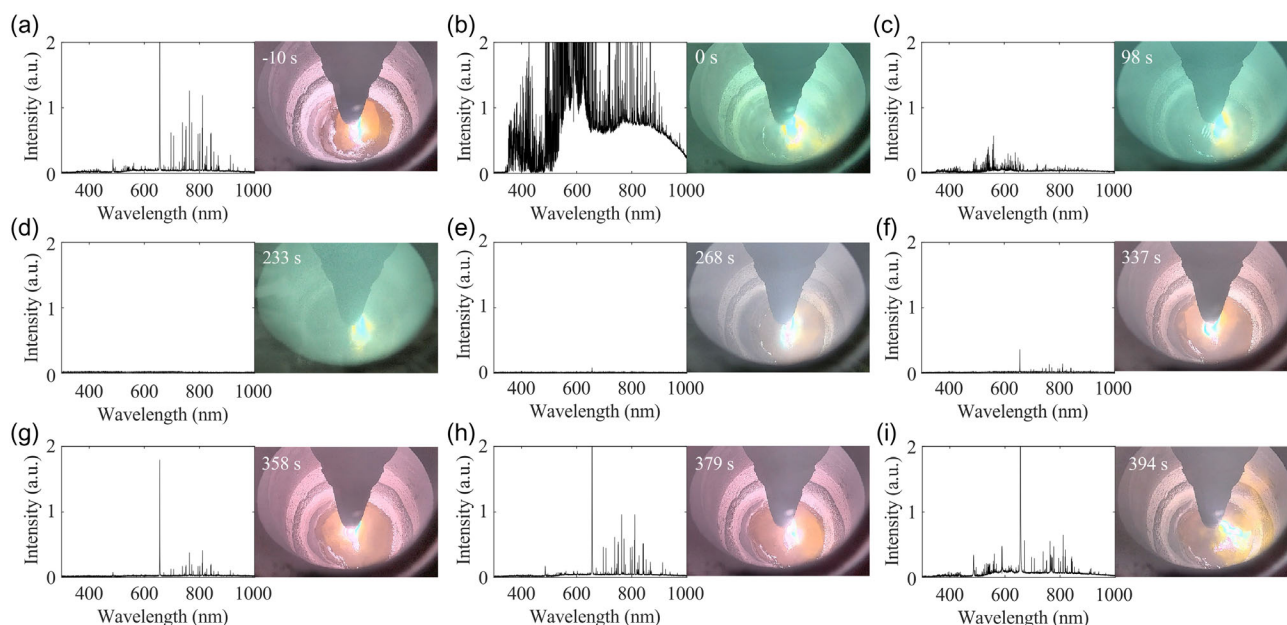


Figure 8. Spectra and images at a) –10 s, b) 0 s, c) 98 s, d) 233 s, e) 268 s, f) 337 s, g) 358 s, h) 379 s, and i) 394 s from the start of the K1-MET experiment 4's continuous charging of fines.

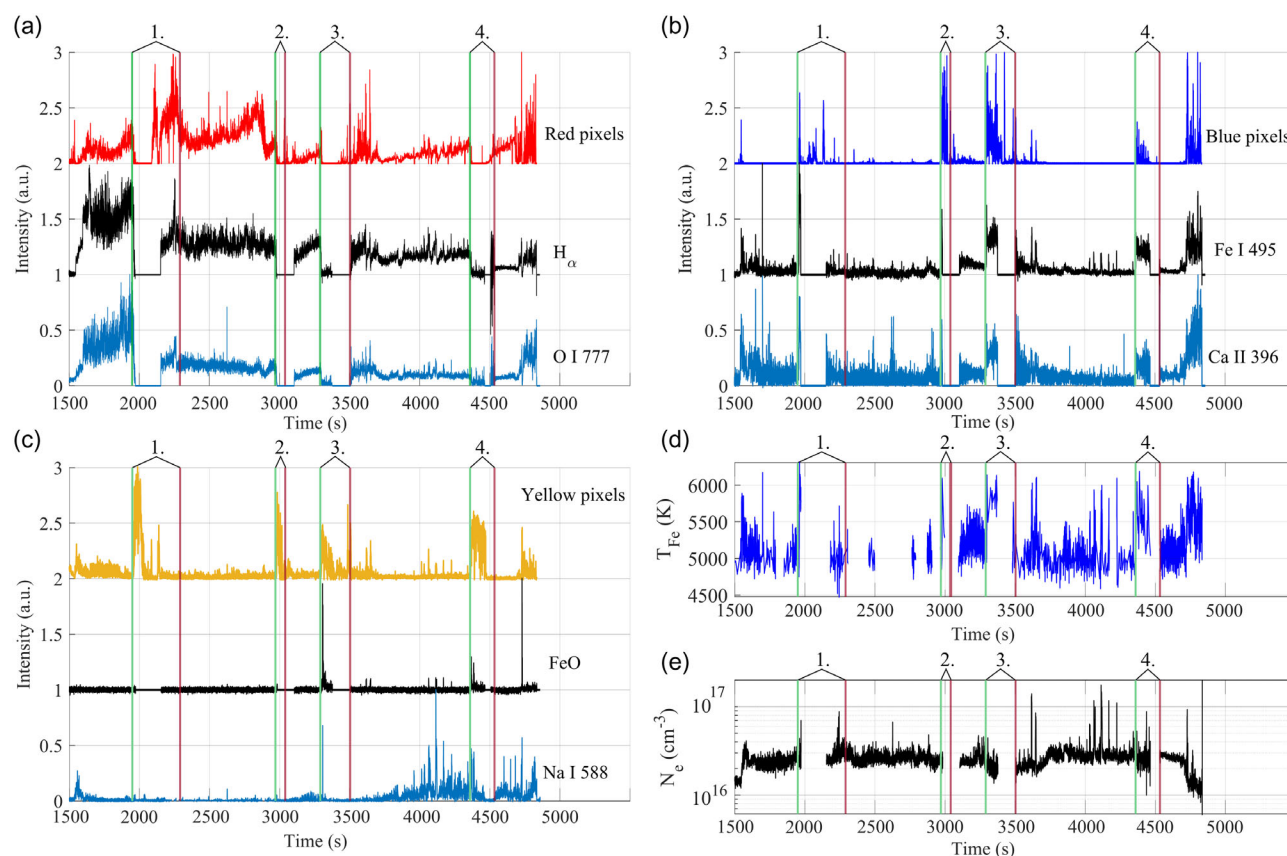


Figure 9. Time evolution of the K1-MET campaign with a) red pixel, H_{α} , and O I intensities, b) blue pixel, Fe I, and Ca II intensities, c) yellow pixel, FeO, and Na I intensities, d) Fe plasma temperature, and e) estimation of electron density with H_{α} . The intensities in (a–c) have been normalized with respect to the overall intensity of the spectrum and an offset has been applied to the graphs for better readability. The continuous charging experiments 1–4 are marked with green (start) and red (finish) vertical lines across the graphs in (a–c).

experiment, temperature increases in all the experiments when the spectra are still seen. The electron density values are problematic during the continuous charging since the H I lines' intensities are very low or not observed at all at these instances. However, outside the continuous charging, electron density has high peaks between 3500 and 4300 s. This aligns well with the increases in Fe I and plasma temperature, where it can be assumed that metallic iron vapor in the plasma leads to higher electron density due to relatively low ionization energy of iron.^[24] At the end when electrode is lifted, the electron density drops due to increasing plasma length. The metallization of the melt was not analyzed because the focus was to study application of OES and image analysis at pilot scale.

4.3. Visibility of the Plasma

The visibility of plasma plays a crucial role in OES applications for HPSR. The plasma must be in the optically accessible cone of view for the optical fiber, and the atmosphere must be optically thin enough for the light to pass through it without interference. During reduction, however, water vapor and dust can cause significant absorption of light throughout the spectral range. **Table 5** summarizes the visibility of plasma in all the experiments investigated in this study. Since the laboratory reduction test at MPIE did not suffer from light absorption, this small-scale reactor is suitable to study both the fundamentals of hydrogen-based plasma metallurgy and the interaction between the plasma and the molten ore without too much disturbing interference from the dust.

The experiments at MUL and K1-MET, on the other hand, had varying degrees of light absorption during the reduction due to dust. In comparison to the MPIE experiments, the mass of material was much larger at MUL and K1-MET, which may have an influence on the higher dust and water vapor formation. When comparing the batch experiment of MUL with the continuous charging of fines at K1-MET, the batch experiments tend to have a clear view of the plasma at the beginning of the experiment and the visibility gradually decreases toward the last few minutes of the experiment. On the contrary, the dust and water vapor

obscure the visibility at the very beginning of the continuous charging. Since the fines are introduced directly into the plasma through the HGE, it is to be expected that the reduction is very intensive when compared to the pellet experiment.

One possibility to increase the light acquisition is to increase the slit width of the spectrometer. This does not come without challenges, as increasing the slit width will broaden the optical emission lines. As shown, for example, in Figure 5 and 8, hundreds of optical emission lines can appear in the spectra. Such a high number of optical emission lines can be a problem in conjunction with broader line width since a wider slit width will make the optical emission lines broader and result in overlapping lines. While this does not necessarily prevent line identification and OES analysis, in-depth plasma analytics that require well-defined line fitting might not be feasible. Another way to increase light acquisition during reduction is to increase the integration time of the spectrometers. This solution was used in the experiments at MUL and K1-MET when the reduction was initiated and manually changed as the light intensity dropped. However, with the chosen spectrometer, increasing the integration time was insufficient during the most intensive dust formation period. Due to the dust's light absorption, an automatic exposure adjustment is recommended for future experiments. As a final note to the spectrometer equipment, the properties of the optical fiber, such as the aperture, can affect the amount of acquired light and should be chosen to suit the experiments in question.

5. Conclusion

This article provides an overview of how OES and color analysis can be used to analyze and monitor the HPSR process of iron ores. The optical spectra and the colors of the plasma provide detailed information about the atoms and molecules radiating within the plasma, where images provide spatial information of the colors in the plasma. The colors can be further analyzed using a spectrometer, revealing information about 1) the composition of the plasma; 2) the characteristics of the plasma, such as

Table 5. Visibility of the plasma for the OES equipment. Green = good visibility, or only a minor fraction of light is absorbed; orange = light is absorbed by the atmosphere, but spectra can still be seen if, for example, integration time is increased; red = view into the reactor is obscured, only the most intense lines, such as alkali and hydrogen, are seen either continuously or from time to time; gray = the experiment does not have the step mentioned in the column title. Some reduction steps varied between good and poor visibility, which are indicated with two colors for a given step.

Laboratory	E	Experiment info	Reduction			
			0–2 min	2–5 min	5–8 min	8–10 min
MPIE	1	10 min, hematite disks, 15.0 g	Green	Green	Green	Green
MUL	1	10 min, pellets, 96.2 g	Green	Green	Orange	Red
Pilot-scale	E	Experiment info	Reduction			
			Charging	3 min after	6 min after	9 min after
K1-MET	1	6 min, 100 g min ⁻¹	Red	Orange	Green	Green
	2	1 min, 100 g min ⁻¹	Red	Green	Gray	Gray
	3	3 min, 100 g min ⁻¹	Orange	Orange	Green	Green
		1 min, 200 g min ⁻¹	Red	Orange	Green	Green
	4	3 min, 100 g min ⁻¹	Orange	Orange	Green	Gray

temperature and electron density; and 3) the spatial distribution of elements in the plasma. In addition to atomic optical emissions, two molecular optical emissions were identified as CaO and FeO. The FeO and atomic iron optical emissions should be investigated in future research since their increasing intensities may be linked to material losses due to evaporation and recombination of FeO molecules.

The observations of this article shed light on how to approach process development and monitoring of HPSR by OES analysis. Hydrogen lines are engulfed by atomic iron during reduction, especially in the beginning, and thus the reappearance of hydrogen lines is an indicator that the reduction process is not as intensive as earlier or it has slowed down. Increasing optical emissions from the gangue elements, such as Ca and CaO, signal that slag has started to form on top of the melt. While OES is a simple and highly effective method to be utilized in HPSR reactors and requires only a direct view of the plasma, the absorption of light by the dust and water vapor that form during the reduction must be considered to ensure that enough light reaches the detector. For this, the authors suggest using a wider spectrometer slit, especially during reduction and increasing the exposure time. The following steps in HPSR OES research are to link the OES and image analyses with the process parameters, such as 1) reduction degree; 2) H₂ and energy consumption; 3) efficiency of the process; and 4) composition of the melt.

Acknowledgements

This work was supported by the Academy of Finland under the Genome of Steel grant no. 311934 and postdoctoral researcher grant no. 349402; Business Finland with the TOCANEM, Towards Carbon Neutral Metals project no. 41700/31/2020; the K1-MET COMET program Fundamentals of hydrogen reduction grant no. 12204396; the Heisenberg-Program of the Deutsche Forschungsgemeinschaft (project number 416498847); and by the European Union through the project ROC, sponsored by the European Research Council ERC through the ERC advanced grant number 101054368. The authors thank Anu Tuomela for practical help with the Andor Solis SR500 spectrometer and the workshop team at MPIE for constructing the necessary adapters required for the optical emission spectroscopy and camera equipment.

Conflict of Interest

The authors declare no conflict of interest.

Data Availability Statement

Data sharing is limited due to the innovation potential and industrial relevance. The data that support the findings of this study may be made available upon reasonable request and consent of all the authors.

Keywords

color analysis, hydrogen plasma smelting reduction, iron ore, optical emission spectroscopy, process monitoring

Received: January 10, 2024

Revised: April 23, 2024

Published online:

- [1] D. Raabe, C. C. Tasan, E. A. Olivetti, *Nature* **2019**, 575, 64.
- [2] European Steel in Figures 2022, <https://www.eurofer.eu/assets/publications/brochures-booklets-and-factsheets/european-steel-in-figures-2022/European-Steel-in-Figures-2022-v2.pdf> (accessed: October 2023).
- [3] H.-J. Odenthal, A. Kemminger, F. Krause, L. Sankowski, N. Uebber, N. Vogl, *Steel Res. Int.* **2017**, 89, 1700098.
- [4] HYBRIT, <https://www.hybritdevelopment.se/en/> (accessed: August 2023).
- [5] J. F. Plaul, W. Krieger, E. Bäck, *Steel Res. Int.* **2005**, 76, 548.
- [6] D. Raabe, *Chem. Rev.* **2023**, 123, 2436.
- [7] M. N. Seftejani, J. Schenk, *Metals* **2018**, 8, 1051.
- [8] I. R. Souza Filho, Y. Ma, D. Raabe, H. Springer, *J. Miner., Met. Mater. Soc.* **2023**, 75, 2274.
- [9] I. R. Souza Filho, Y. Ma, M. Kulse, D. Ponge, B. Gault, H. Springer, D. Raabe, *Acta Mater.* **2021**, 213, 116971.
- [10] M. A. Zarl, M. A. Farkas, J. Schenk, *Metals* **2020**, 10, 1394.
- [11] D. Ernst, U. Manzoor, I. R. Souza Filho, M. A. Zarl, J. Schenk, *Metals* **2023**, 13, 558.
- [12] I. R. Souza Filho, H. Springer, Y. Ma, A. Mahajan, C. C. da Silva, M. Kulse, D. Raabe, *J. Cleaner Prod.* **2022**, 340, 130805.
- [13] M. A. Zarl, D. Ernst, J. Cejka, J. Schenk, *Materials* **2022**, 15, 4767.
- [14] D. Ernst, M. A. Zarl, J. Cejka, J. Schenk, *Materials* **2022**, 15, 4065.
- [15] M. Naseri Seftejani, J. Schenk, D. Spreitzer, M. A. Zarl, *Materials* **2020**, 13, 935.
- [16] P. R. Behera, B. Bhoi, R. K. Paramguru, P. S. Mukherjee, B. K. Mishra, *Metall. Mater. Trans. B* **2019**, 50, 262.
- [17] D. Ernst, M. A. Zarl, M. A. Farkas, J. Schenk, *Steel Res. Int.* **2023**, 94, 2200818.
- [18] H. Pauna, M. Aula, M. Huttula, T. Fabritius, *Steel Res. Int.* **2021**, 93, 2100519.
- [19] H. Pauna, M. Aula, J. Seehausen, J.-S. Klung, M. Huttula, T. Fabritius, *Steel Res. Int.* **2021**, 91, 2000051.
- [20] H. Pauna, D. Ernst, M. A. Zarl, M. Aula, J. Schenk, M. Huttula, T. Fabritius, *J. Cleaner Prod.* **2022**, 372, 133755.
- [21] A. Kramida, Y. Ralchenko, J. Reader, N. A. Team, NIST Atomic Spectra Database, <https://www.nist.gov/pml/atomic-spectra-database> (accessed: August 2023).
- [22] P. Julien, S. Whiteley, S. Goroshin, M. Soo, D. Frost, J. Berghartson, *Proc. Combust. Inst.* **2015**, 35, 2431.
- [23] D. Surmick, C. Parigger, *Int. Rev. At. Mol. Phys.* **2014**, 5, 73.
- [24] A. Gleizes, Y. Cressault, *Plasma Chem. Plasma Process.* **2017**, 37, 581.